Acoustic Emission Measurement of a Wind Turbine Main Bearing

Yi Guo,[1] Allan Thomson,[2] Roger Bergua,[1] Olle Bankestrom,[2] Joe Erskine,[2] and Jonathan Keller[1]

1 National Renewable Energy Laboratory
2 SKF

NREL is a national laboratory of the U.S. Department of Energy
Office of Energy Efficiency & Renewable Energy
Operated by the Alliance for Sustainable Energy, LLC

This report is available at no cost from the National Renewable Energy Laboratory (NREL) at www.nrel.gov/publications.

Contract No. DE-AC36-08GO28308

Technical Report
NREL/TP-5000-83370
October 2022

Acoustic Emission Measurement of a Wind Turbine Main Bearing

Yi Guo,[1] Allan Thomson,[2] Roger Bergua,[1] Olle Bankestrom,[2] Joe Erskine,[2] and Jonathan Keller[1]

1 National Renewable Energy Laboratory
2 SKF

Suggested Citation
Guo, Yi, Allan Thomsen, Roger Bergua, Olle Bankestrom, Joe Erskine, and Jonathan Keller. 2022. *Acoustic Emission Measurement of a Wind Turbine Main Bearing*. Golden, CO: National Renewable Energy Laboratory. NREL/TP-5000-83370.
https://www.nrel.gov/docs/fy23osti/83370.pdf

NREL is a national laboratory of the U.S. Department of Energy
Office of Energy Efficiency & Renewable Energy
Operated by the Alliance for Sustainable Energy, LLC

This report is available at no cost from the National Renewable Energy Laboratory (NREL) at www.nrel.gov/publications.

Contract No. DE-AC36-08GO28308

Technical Report
NREL/TP-5000-83370
October 2022

National Renewable Energy Laboratory
15013 Denver West Parkway
Golden, CO 80401
303-275-3000 • www.nrel.gov

NOTICE

This work was authored in part by the National Renewable Energy Laboratory, operated by Alliance for Sustainable Energy, LLC, for the U.S. Department of Energy (DOE) under Contract No. DE-AC36-08GO28308. Funding provided by the U.S. Department of Energy Office of Energy Efficiency and Renewable Energy Wind Energy Technologies Office. The views expressed herein do not necessarily represent the views of the DOE or the U.S. Government.

This report is available at no cost from the National Renewable Energy Laboratory (NREL) at www.nrel.gov/publications.

U.S. Department of Energy (DOE) reports produced after 1991 and a growing number of pre-1991 documents are available free via www.OSTI.gov.

Cover Photos by Dennis Schroeder: (clockwise, left to right) NREL 51934, NREL 45897, NREL 42160, NREL 45891, NREL 48097, NREL 46526.

NREL prints on paper that contains recycled content.

List of Acronyms

AEE	acoustic emission enveloping
DVST	design verification support tool
kN	kilonewton
kW	kilowatt
m/s	meters per second
MW	megawatt
NREL	National Renewable Energy Laboratory
Pk2Pk	peak to peak
rpm	revolutions per minute
RMS	root-mean-square

Table of Contents

List of Figures

List of Tables

1 Introduction

In most wind turbines, one or more rolling element bearings are used to support the rotor weight and aerodynamic forces and moments and thus are called the “main” bearings. Main bearings do not have an application-specific design standard and are typically rated with respect to International Organization for Standardization standards, technical specifications, or supplier specifications for a modified reference rating life with 90% survival probability, as described in International Electrotechnical Committee standard 61400-1 (Keller et al. 2021; Nejad et al. 2022). However, premature, nonrolling contact fatigue main bearing failures (Kotzalas and Doll 2010; Brake 2013; Greco et al. 2013; Hart et al. 2019, 2020; Chovan and Fierro 2021; Keller et al. 2021) have been observed, in some populations with failure rates as high as 20%–30% in as little as 6–10 years (Brake 2013; Sethuraman, Guo, and Sheng 2015; Hart et al. 2019). Removal and replacement of a main bearing typically requires rotor removal with a crane and results in appreciable maintenance costs and downtime.

In December 2017, a specially instrumented, commercial main bearing, main shaft, and gearbox were installed in a General Electric 1.5-megawatt (MW) SLE turbine at the National Renewable Energy Laboratory (NREL) Flatirons Campus. The purpose of the instrumentation and testing program was to understand operational conditions suspected of being related to premature main bearing and gearbox failures. Over 3 years of data were collected (Keller, Guo, and Sethuraman 2019) before decommissioning most of the main bearing and gearbox instrumentation in August 2021. Thus far, the analysis has examined the relationship between main bearing axial motion and expected lubrication characteristics. We found the axial velocity of the rollers compared to their rolling speed to be negligible and thus not expected to influence lubricant film thickness (Guo et al. 2021). Main bearing loads, including those induced by gravity, aerodynamic rotor thrust and side loads, and pitch and yaw moments, are the result of interactions between the rotor and the complex wind field in which it is operating (Hart et al. 2020, 2022; Hart 2020). Typical main bearing loads and the resulting roller-load-induced strain of the bearing were also examined for evidence of cage slip and for predicting roller loads and contact stresses. No evidence of cage slip was found and contact stresses up to 2 gigapascals were predicted at the rated turbine condition (Bergua Archeli et al. 2021).

This report continues the examination of main bearing operational conditions by examining additional measurements related to the condition of its lubricant film. Proper lubrication of the main bearing is essential to separate bearing internal surfaces and minimize wear (Hart, de Mello, and Dwyer-Joyce 2021a). Indeed, the fatigue life assessment process for rolling bearings explicitly assumes that proper lubrication conditions hold throughout the bearing lifetime (Hart et al. 2020). The lubricant and lubrication mechanisms are therefore fundamental to main-bearing operation and lifetime; therefore, they must be considered to properly investigate possible damage mechanisms (Hart, de Mello, and Dwyer-Joyce 2021b).

2 Test Article and Instrumentation

The GE 1.5 SLE research turbine was installed and commissioned at the NREL Flatirons Campus in September 2009. In December 2017, the main bearing, main shaft, and gearbox were replaced to facilitate several drivetrain tests, including on the main bearing (Keller, Guo, and Sethuraman 2019). The newly developed main bearing, shown in Figure 1, is an SKF model BS2-8115/C2H spherical roller bearing lubricated with SKF Winter Grade LGWM2 grease (SKF 2022a). Although it is similar to a standard 240/600 ECA/W33 double-row SKF Explorer series spherical roller bearing with a bore diameter of 600 millimeters (mm) and width of 272 mm, the installed main bearing has only 28 rollers in each row. Its design was updated to optimize internal geometry specific to the wind turbine loads, use a new cage design and material, provide better sealing through a customized seal design, and improve lubrication with an automated relubrication system (Raju and Bankestrom 2017; James 2018). This bearing now has the commercial designation 240/600 BC (SKF 2022b). The main bearing, auxiliary equipment, and some of the instrumentation were contributed to the project by SKF USA under cooperative research and development agreement CRD-17-702. During its first 2 years of operation, the main bearing was inspected twice and the grease was sampled approximately every 6 months. Borescope images of the load zone taken during the second year of operation showed that the rollers (running surface and ends), cage, and inner and outer raceways were all in good condition. By February 2021, the drivetrain had accumulated 2,279 operating hours (Guo et al. 2021).

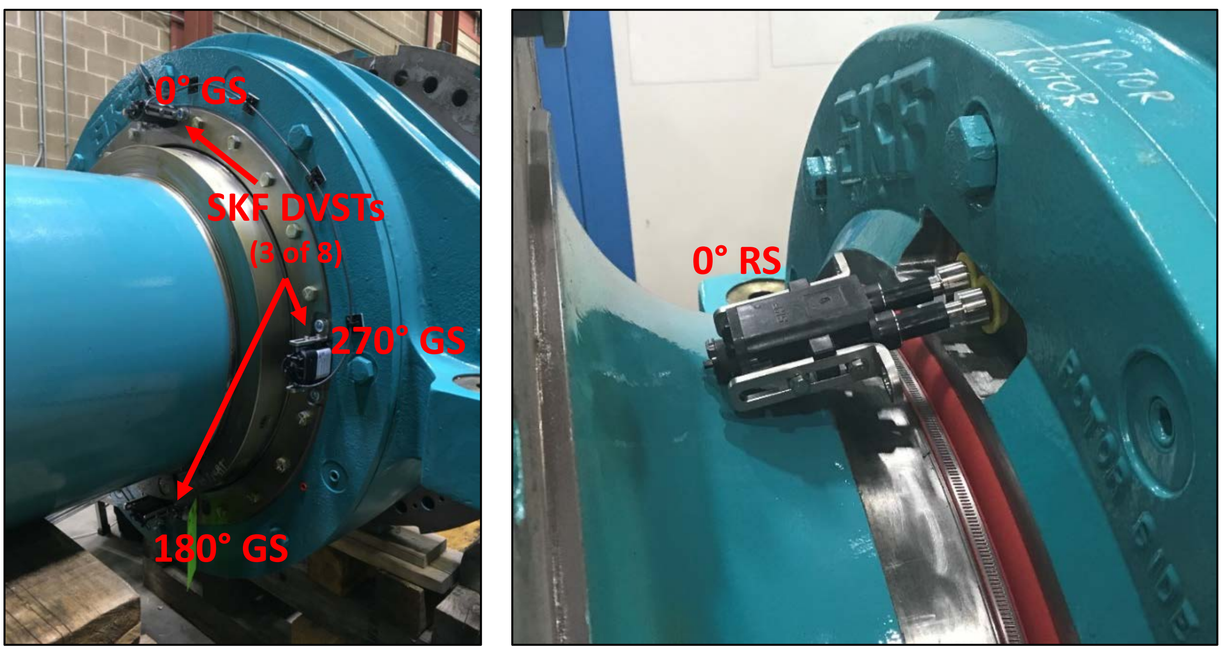

Figure 1. Example generator-side (left) and rotor-side (right) design verification support tool nodes. *Photos by Jonathan Keller and Mark Dunn, NREL 49379 and 65814*

The primary subject of this report is the examination of measurements from the design verification support tool (DVST) nodes provided by SKF, also shown in Figure 1. Eight DVST nodes, split evenly on the rotor side and generator side of the main bearing are installed at four locations around the bearing circumference (0°, 90°, 180°, and 270° when viewed from the rotor side). The DVST nodes are bolted to a specially machined recess on the bearing cover. When the

DVST node is mounted, its two spring-loaded legs protrude through the machined holes in the cover and contact the side face of the stationary bearing outer ring. The tip of one leg measures the tangential strain through a contact strain gauge, whereas sensors on the other tip measure acoustic emission, vibration, and temperature. Ideally, the contact force and friction between the legs and the side face of the stationary outer ring are sufficient to measure these quantities. An O-ring around the tip of each leg helps prevent external contamination, such as by bearing grease. The rotational speed of the main shaft is measured by a ninth, unmounted DVST node and a separate tachometer (Bergua Archeli et al. 2021). Previous work examined the tangential strain characteristics (Bergua Archeli et al. 2021). Axial vibration is primarily used for bearing condition monitoring, so it is not examined herein. This report examines characteristics of the acoustic emission and temperature as correlated to the wind turbine operating conditions, including wind speed, rotor speed, rotor loads, and active power.

Acoustic emissions can occur at frequencies between tens of kilohertz and 1 or 2 megahertz (Hase, Mishina, and Wada 2012; Fuentes et al. 2020), much higher than measurable by most vibration transducers. As a result, acoustic emission sensors can detect transient elastic surface waves created by plastic deformation of materials, by crack initiation and propagation, by frictional sources, and throughout the wear process. Acoustic emissions have a much greater sensitivity to incipient bearing defects when compared to vibration due to its enhanced signal-to-noise ratio (Hase, Mishina, and Wada 2012; Cockerill et al. 2016). Acoustic emissions can also be interpreted to assess the lubrication condition of gears and rolling element bearings, asperity interactions, and other bearing- and machine-related anomalies such as contamination, fluting, fretting, bearing cracks, skidding, and smearing (SKF 2014; Hutt, Clark, and Evans 2018; Fuentes et al. 2020; Cornel et al. 2021). Asperity contacts can create micro-welds, which when broken produce acoustic stress waves. Bearing faults and other sources also result in stress events that can produce similar stress waves in the bearing. The resulting frequency of stress wave oscillations is the carrier signal, which is modulated at the instances that the stress waves occur, as shown in Figure 2.

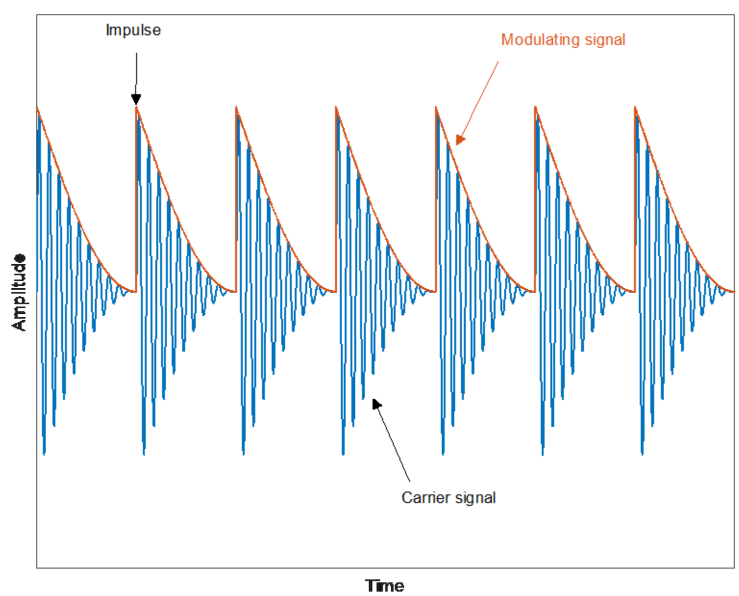

Figure 2. Signal modulation and processing

Asperity contacts tend to create aperiodic (i.e., pseudo-random) modulation, whereas bearing faults, gear mesh excitations, and blade passage tend to create periodic modulation. Experience has shown that in a more complex environment like a wind turbine drivetrain the surrounding components (e.g., blade passage, bolted connections, gearbox) can also create acoustic emissions, which complicates this interpretation. Because of this, analyzing acoustic emissions typically must consider any signal periodicity to help determine the source in addition to the signal magnitude.

A DVST node measures acoustic emissions and then band-pass filters them between 100,000 and 500,000 hertz, rectifies, and envelopes (i.e., demodulates) them through signal conditioning hardware in a method called acoustic emission enveloping (AEE) (SKF 2014). These AEE data are recorded for a duration of 32 seconds (s) at 256 hertz, typically once every 5 minutes. DVST node measurements can also be commanded by the user. The acquisition of DVST node measurements can be configured, but not all measurements can be simultaneously acquired. For this test, the quantities in Table 1 are recorded at times when the main shaft rotational speed is between specified minimum and maximum rotational speeds. Only one DVST node, at the 0° rotor-side circumferential position, was used to measure AEE.

Table 1. DVST Nodes and Measurements

Signal Name	Circumferential Position	Temperature (°C)	Axial Acceleration Enveloping (g)	Tangential Strain (με)	Acoustic Emission Enveloping (-)
12_UW	0° rotor side	X			X
3_UW	90° rotor side	X	X		
6_UW	180° rotor side	X		X	
9_UW	270° rotor side	X	X		
12_DW	0° generator side	X		X	
3_DW	90° generator side	X		X	
6_DW	180° generator side	X		X	
9_DW	270° generator side	X		X	

g = acceleration due to gravity, με = microstrain

Bearing temperature and main shaft speed are also important considerations because they relate to the viscosity and film thickness of the lubricant. Previous simulations of a 1.5-MW wind turbine showed mixed lubrication conditions occurring in the worst-case conditions (i.e., lower speeds, higher temperatures, more grease starvation) (Hart, de Mello, and Dwyer-Joyce 2021b). Mixed lubrication conditions are a state in which some penetration of the lubricant film has occurred, such that the load is shared between asperity contacts and fluid pressures. For this test, bearing temperature measurements were acquired by all eight DVST nodes mounted on the main bearing.

The DVST node measurements are recorded by a personal computer located in the nacelle with the corresponding time for accurate data timestamping and system clock setting, which is especially useful for correlating with the other collected meteorological and turbine operational parameters (Santos and van Dam 2015; Keller, Guo, and Sethuraman 2019). DVST node data are transferred via a cellular connection to a cloud server. The collected DVST data are then merged with the wind turbine's operational parameters and meteorological information, including wind speed, active power, blade pitch angle, and turbine loads to enable the correlation study described in the next section.

3 Data Analysis Results and Discussion

The primary purpose of the analysis described in this section is to examine any correlation between the wind turbine operating condition and characteristics of the AEE data; and thus, by extension, insight into the main bearing lubrication condition, potential evidence of any asperity interactions, or presence of other acoustic emission sources. A total of 2,462 AEE data sets collected from November 2018 to March 2019 were included in this study, which is the same time period as the bearing tangential strain measurement study (Bergua Archeli et al. 2021).

3.1 Description of AEE Data

Two example, 32-s AEE time waveforms recorded by the 0° rotor-side DVST node are shown in Figure 3. These two data samples were collected at average wind speeds of 5 meters per second (m/s), in which the turbine is operating well below rated rotor speed and power, and 16 m/s, in which the turbine is operating at rated rotor speed and power. At 5-m/s wind speed, the waveform is nearly flat, with fluctuations of about 1. At 16-m/s wind speed, the waveform has a similar median value but many distinct spikes with magnitudes of 10 to over 100. In addition, these waveforms have a nonzero median and some negative values, which as expected is related to the signal conditioning process through hardware. The occurrence of these spikes may or may not be random. Random spikes may indicate potential asperity contact in the main bearing or other sources of acoustic emission. Periodic spikes may indicate bearing damage or also other sources acoustic emission. Within the 5-month data set, 32% of the AEE data records include such spikes whereas 68% of them do not. As discussed earlier, the turbine has only accumulated 2,279 operating hours and the main bearing is in good condition. Thus, these spikes might be caused by asperity contacts related to wind turbine operating conditions and/or other acoustic emission sources, such as the gearbox, bolted connections, and blades.

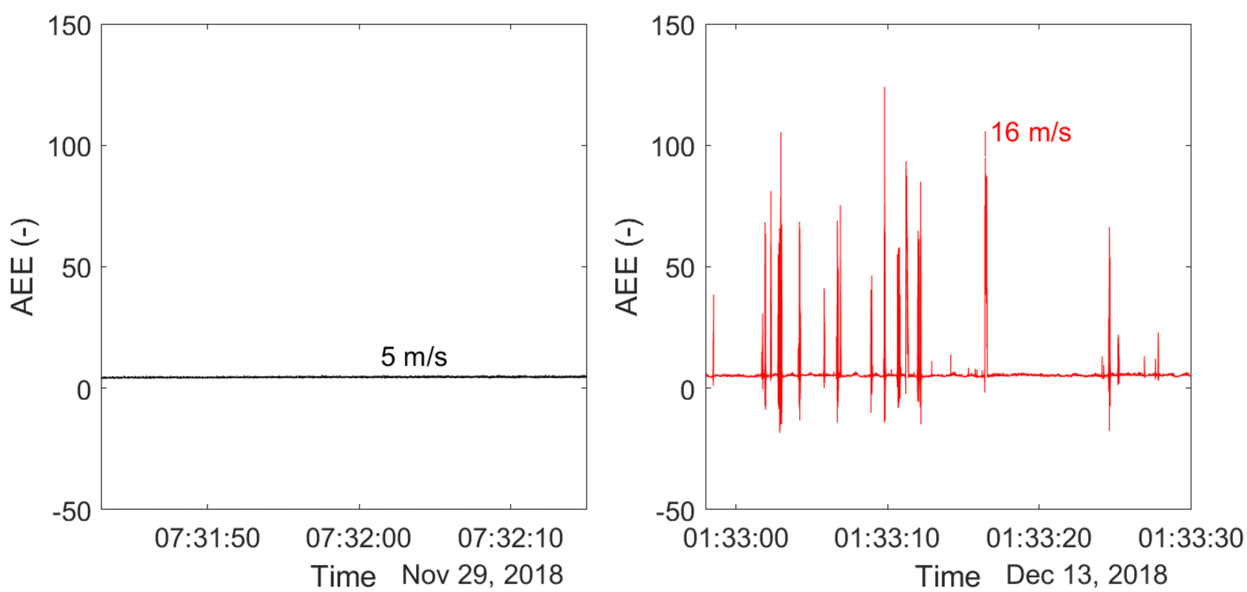

Figure 3. Example AEE measurements at 5-m/s (left) and 16-m/s (right) wind speeds

This AEE time waveform can be further post-processed into several indicators of interest, such as the peak-to-peak (Pk2Pk), root-mean-square (RMS), and number of acoustic events (number of spikes). The RMS is calculated after subtracting the median value from the waveform to remove any residual offset from zero in the signal. Spikes in the AEE time waveform are identified when any value is 2 higher than the median. The Pk2Pk is then the average value of the difference between the magnitudes of the identified spikes and the median. These indicators can change with the bearing rotational speed and the lubricant viscosity ratio (itself strongly influenced by bearing temperature), but less so with applied load (SKF 2014; Cockerill et al. 2016). For a grease-lubricated bearing in good mechanical condition and sufficient lubrication film (i.e., lubricant viscosity ratio between 1 and 5), the acoustic emission enveloping RMS is generally under 3 or even 2 depending on the speed, temperature, and load. In situations where the lubricant film becomes thinner and asperity contact between the rollers and raceway begins, the acoustic emission enveloping Pk2Pk can increase from values below 1 to an order of magnitude or more (tens to hundreds), depending on the bearing speed, as the asperity contacts increase in frequency and severity (SKF 2014). At 5 m/s, the RMS is 0.2 and the Pk2Pk is 0, whereas at 16 m/s the RMS is 5.4 and the Pk2Pk is 21.2. Other indicators in the AEE time waveform can indicate changes in viscosity or even the presence of water in the grease. However, AEE measurements and the boundaries of interpretation change significantly from application to application depending on attenuation factors, levels of background acoustic emissions and the rolling contact speeds within the bearing. Comparisons to a healthy baseline and trending are essential (SKF 2014; Cockerill et al. 2016).

3.2 Correlation of AEE Data and Wind Speed

A broader statistical analysis of the acoustic emission enveloping RMS over the full operating envelope of the turbine from the cut-in (3 m/s) to cut-out (25 m/s) wind speed is described in this section. Figure 4 shows the blade pitch angle, rotor speed, and active power. The pitch angle remains near zero below the rated wind speed of 11 m/s and increases to up to 27° at the highest wind speeds. The rotor speed rises quickly from 11 revolutions per minute (rpm) at the lowest wind speeds and reaches the rated rotor speed of 18.4 rpm at an approximate wind speed of 7 m/s. When the wind speed is within this range, the rotor speed can naturally change by a significant amount in a 32 s data sample. Above that point, the rotor speed remains relatively close to its rated value, only varying by about ±3%. Active power reaches the rated value of 1,500 kilowatts (kW) at the rated wind speed but does vary as much as ±15% above the rated wind speed. These observed behaviors are as expected from previous drivetrain measurement campaigns (Keller, Guo, and Sethuraman 2019; Guo et al. 2021).

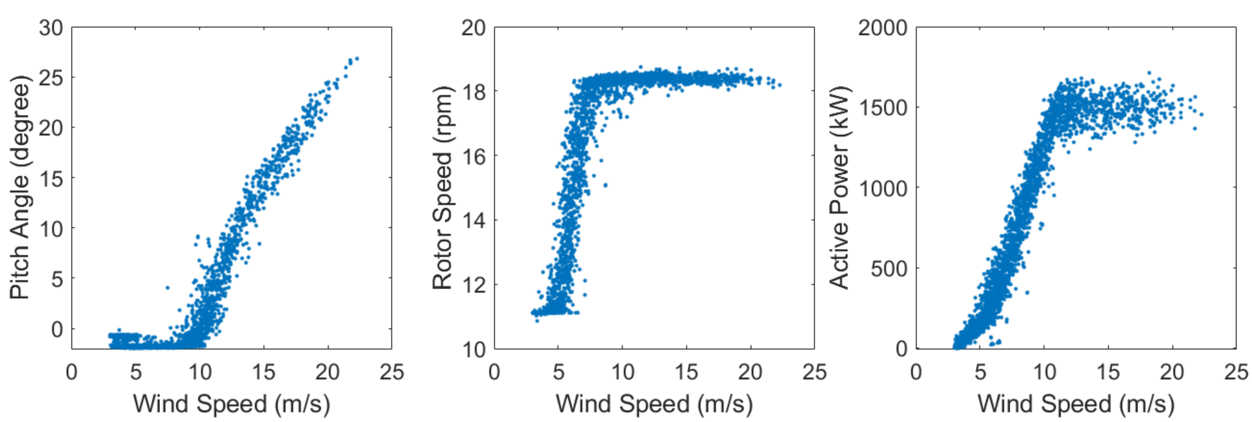

Figure 4. Variation of blade pitch angle (left), rotor speed (middle), and active power (right) with wind speed

The correlation between wind speed and the AEE indicators (RMS, Pk2Pk, and number of spikes) is shown in Figure 5, with the moving average of each displayed in green. The RMS increases with wind speed and reaches a maximum at about 14 m/s, which is above the rated wind speed. Beyond this point, the acoustic emission enveloping RMS decreases. The elevated RMS values are primarily a result of increased number and magnitude of spikes—at 14 m/s there were up to 700 spikes detected with Pk2Pk values (i.e., average magnitudes) of 30. With many RMS values above the normal value of 3, it is clear that acoustic emissions from either asperity contacts or other sources are being measured in these conditions. The following sections will study the correlation between the wind turbine operating parameters and the AEE characteristics separately.

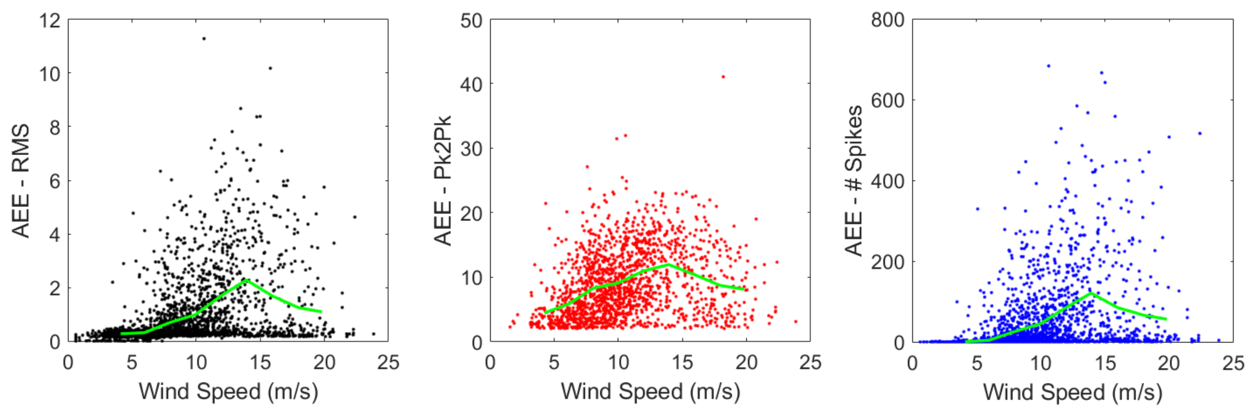

Figure 5. Variation of acoustic emission enveloping RMS (left), Pk2Pk (center), and number of spikes (right) with wind speed

3.3 Correlation of AEE Data and Primary Operating Parameters

Driven by constantly changing environmental conditions, wind turbines operate at various rotor speeds, temperatures, and loads. These operating parameters are the primary ones that are expected to have the greatest impacts on the AEE data. However, they can vary simultaneously, so it is almost impossible to distinguish their individual effects. The following discussion studies the correlation between these primary operating parameters and the AEE data and discusses their influences qualitatively.

3.3.1 Rotor Speed

The correlation between rotor speed and the AEE indicators (RMS, Pk2Pk, and number of spikes) is shown in Figure 6, with the moving average displayed in green. The indicators all remain relatively low below a rotor speed of 18 rpm, at which the wind speeds are less than 7 or 8 m/s and the active power is less than 400 kW. In these conditions, the rotor speed is lower than in rated conditions, so naturally there are fewer measured spikes in a 32 s data set. Above this point, the AEE indicators can all vary by a significant amount as does the wind speed, pitch angle, power, and other loads.

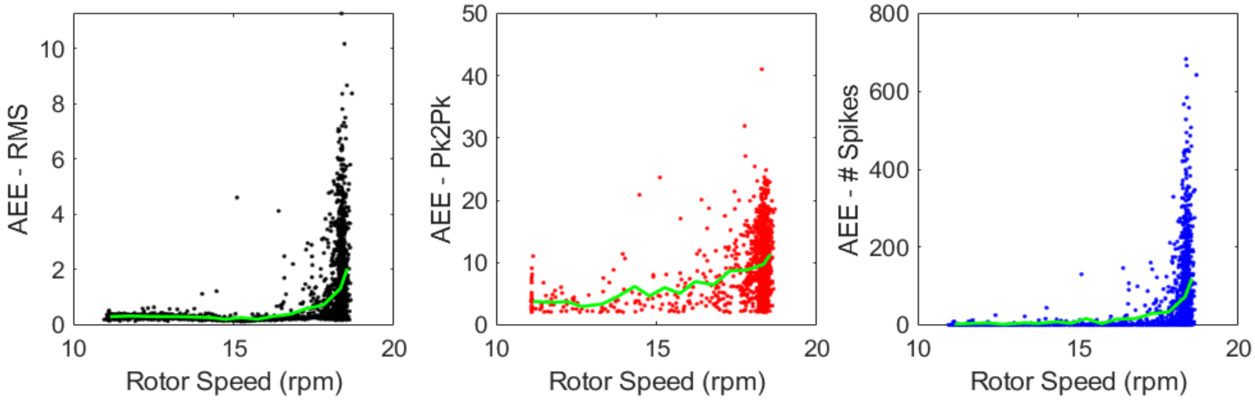

Figure 6. Variation of acoustic emission enveloping RMS (left), Pk2Pk (center), and number of spikes (right) with rotor speed

3.3.2 Bearing Temperature

Operational temperatures of healthy main bearings are typically between 20 and 40 °C, with higher temperatures occurring when a fault develops (Beretta et al. 2021; de Mello et al. 2021). Figure 7 shows the bearing outer-ring side face temperature measured by all eight DVST nodes compared to the outside ambient and nacelle air temperatures. During this winter 2018 measurement campaign, the bearing side face temperatures ranged from 10°C to 34°C, approximately 20 to 25°C higher than the ambient temperature. Therefore, these bearing temperatures are anticipated to be higher during the summer, when the ambient temperatures can reach approximately 30°C.

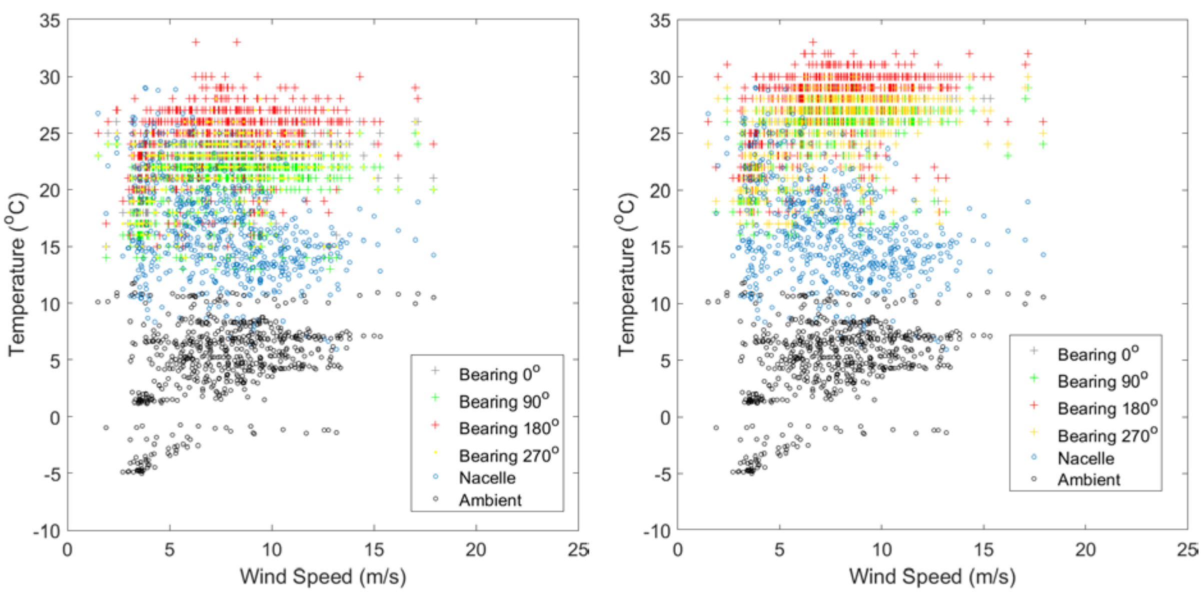

Figure 7. Rotor-side (left) and generator-side (right) bearing outer-ring-side face temperatures

Figure 8 compares the temperatures for both bearing rows near the rated wind speed. In this condition, the generator-side row is fully loaded around its circumference, with the highest load occurring at the 180° position, and the rotor-side row is unloaded because of the rotor thrust (Bergua Archeli et al. 2021). Because of this loading, the generator-side row is 4°C warmer than the rotor-side row and the temperature at the 180° position is higher than the other circumferential locations.

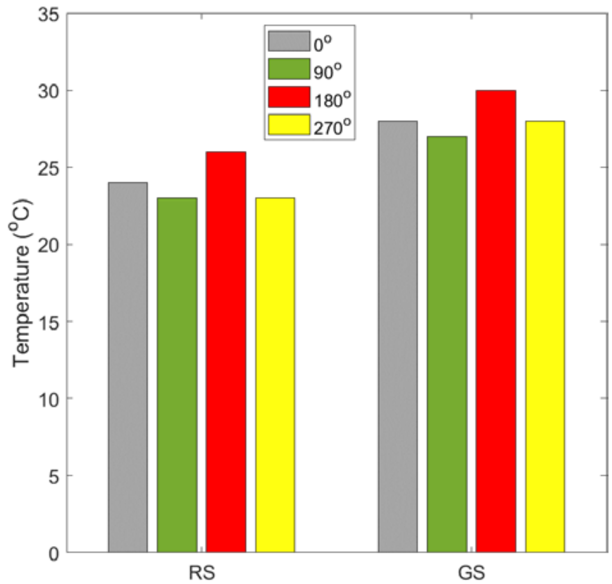

Figure 8. Bearing outer-ring-side face rotor-side and generator-side temperatures at 12-m/s wind speed

The correlation between bearing temperature and the AEE indicators is shown in Figure 9. All three AEE indicators (RMS, Pk2Pk, and number of spikes) typically increase with rising bearing temperature. For a constant bearing load and speed, an increase in the bearing temperature will decrease the lubricant viscosity and, as a result, reduce the lubricant film thickness. Lubrication condition, specifically the lubricant viscosity ratio κ, can be calculated based on SKF's online tool. Most bearing applications are designed for a lubrication condition ranging from $\kappa = 1$ to 4 (SKF 2022c). For this application at rated wind speed and rated rotor speed, κ is between 1 and 2.3 at bearing temperatures of 30°C and 20°C, respectively. At cut-in wind speed and the corresponding rotor speed, κ is between 0.5 and 1.6 for the same bearing temperature range. Overall, κ can be between 0.5 and 2.3 during wind turbine operations. Values of κ between 0.1 and 4 indicate mixed lubrication conditions and potential asperity contacts between the rollers and raceways. Because the bearing is typically not operating with full film thickness, the increase of the AEE indicators shown in Figure 9 might reflect the disturbance of lubricant film thickness with rising temperature.

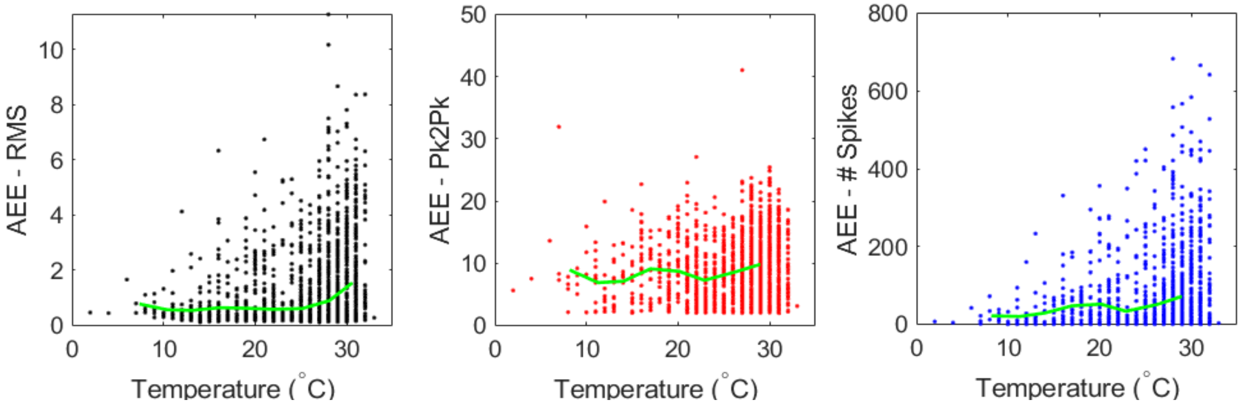

Figure 9. Variation of RMS (left), Pk2Pk (center), and number of spikes (right) with bearing outer-ring-side face temperature

3.3.3 Bearing Loads

The main bearing is subjected to significant radial and axial loads. In this three-point mount drivetrain configuration, the dominant radial load is a result of the rotor weight itself, the rotor weight moment about the main bearing as balanced by the gearbox mounts, and any aerodynamic loads. The dominant axial load is the aerodynamic rotor thrust and some of the rotor weight as a result of the drivetrain tilt. In idling conditions, the total bearing load is shared almost equally between the rotor-side and generator-side rows and the bearing is resting near the center of its axial clearance. As the wind speed and aerodynamic rotor thrust increases, the main shaft and bearing inner ring shift quickly in the downwind direction through the axial clearance. By the time the wind speed reaches rated, the total bearing load is entirely supported by the generator-side row, which is fully loaded circumferentially. This axial motion, both in terms of displacement and velocity, is relatively small and the effect on lubrication film was deemed negligible. It is worth noting that the radial load is also changing with wind speed, typically decreasing as the aerodynamic pitch moment increases caused by wind shear and unloads the rotor weight moment (Guo et al. 2021; Bergua Archeli et al. 2021).

We used measurements of the rotor pitch and tower base moments to estimate the aerodynamic rotor thrust reacted by the main bearing. The aerodynamic pitch moment at the hub center can then be derived from the blade root loads or those measured on the main shaft (Guo et al. 2021). Figure 10 shows the axial load on the main bearing, including rotor aerodynamic thrust and the contribution from the rotor weight, as a function of wind speed. The axial load increases with wind speed quickly from cut-in to rated wind speed, at which it reaches a peak mean value of approximately 250 kilonewtons (kN). Above rated wind speed, the axial load gradually decreases caused by blade pitching and levels off above 20-m/s wind speed.

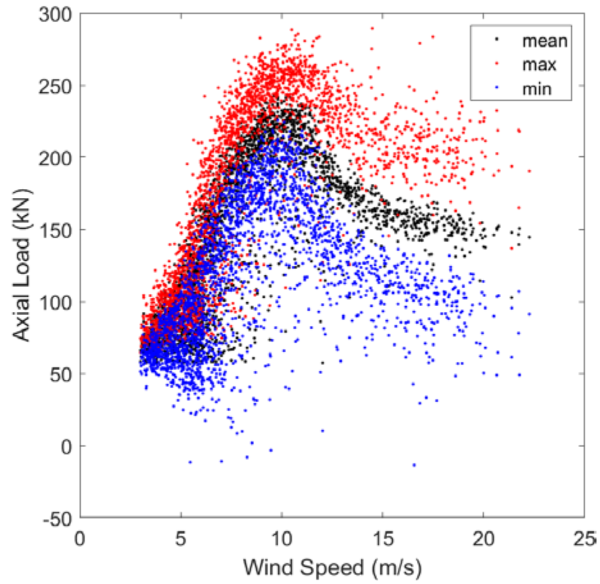

Figure 10. Variation of axial load with wind speed

The correlation between the mean axial load and the AEE indicators is shown in Figure 11. The AEE indicators (RMS, Pk2Pk, and number of spikes) are all low under a mean axial load of 150 kN, which corresponds to wind speeds below 7 or 8 m/s and rotor speeds well below rated. The AEE indicators tend to reach their highest values at mean axial loads between 150 and 225 kN, which corresponds to a small portion of wind speeds just below rated—from 8 to 9 m/s—and to the highest wind speeds—from 14 m/s and up to the cut-out at 25 m/s. Both of these conditions occur at the rated rotor speed. However, as shown earlier in Figure 4, it is likely that the majority of these high AEE values occur around a wind speed of 14 m/s. The AEE indicators actually tend to decrease as the mean axial load approaches the peak of 250 kN, which occurs only near the rated wind speed of 11 m/s and at the rotor speed.

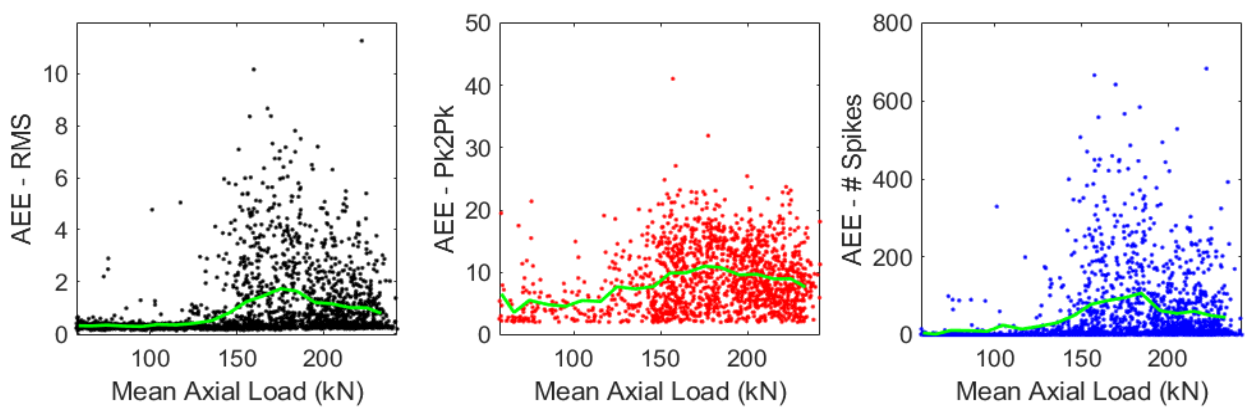

Figure 11. Variation of AEE RMS (left), Pk2Pk (center), and number of spikes (right) with mean axial load

3.4 Correlation of AEE Data and Other Operating Parameters

3.4.1 Active Power

The correlation between active power and the AEE indicators is shown in Figure 12. The AEE indicators (RMS, Pk2Pk, and number of spikes) increase with active power and reach their maximums at the turbine rated power. The AEE RMS values stay relatively low and constant when power is less than 400 kW. Active power is a function of rotor speed and torque. As shown earlier in Figure 4, the rotor speed reaches rated when the wind speed reaches 7 or 8 m/s and the active power reaches 400 kW. Above that point the rotor speed is constant and torque increases as the wind speed rises.

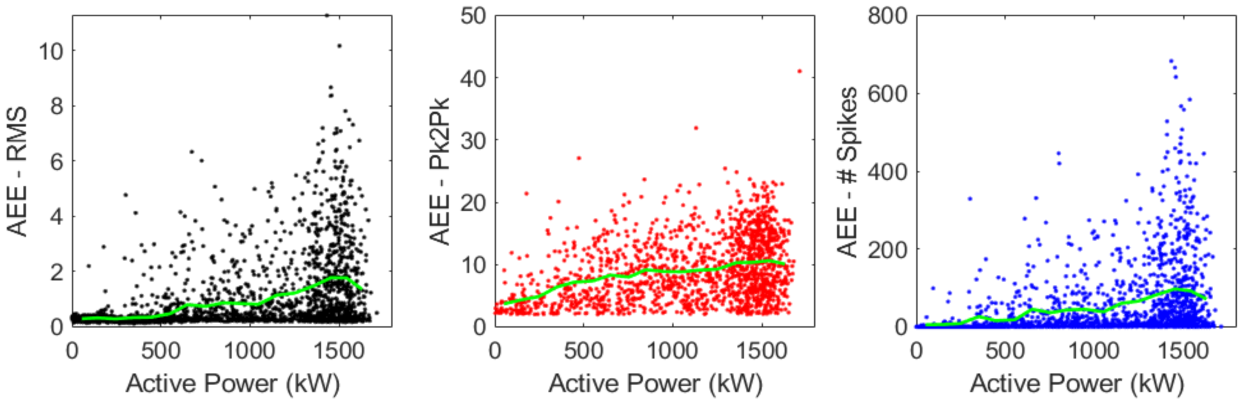

Figure 12. Variation of acoustic emission enveloping RMS (left), Pk2Pk (center), and number of spikes (right) with active power

3.4.2 Pitch Angle

The correlation between the blade pitch angle and the AEE indicators is shown in Figure 13. The acoustic emission enveloping indicators (RMS, Pk2Pk, and number of spikes) do not appear to have any obvious correlation with pitch angle. The highest values occur at pitch angles of approximately 8 to 12 degrees.

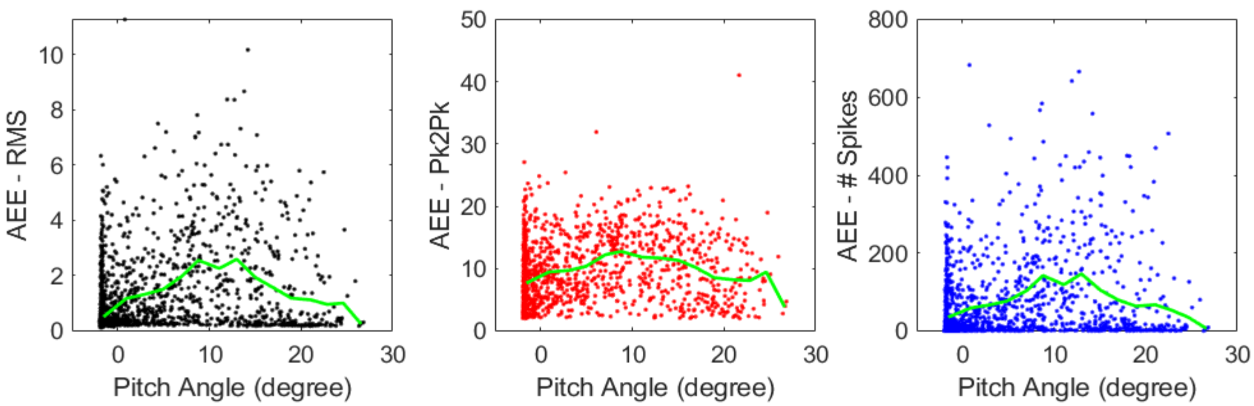

Figure 13. Variation of acoustic emission enveloping RMS (left), Pk2Pk (center), and number of spikes (right) with pitch angle

3.5 Discussion of Other Acoustic Emission Sources

The measured AEE data are likely affected by acoustic emission sources other than from the main bearing itself, consisting of broadband acoustic emissions caused by the interaction of flow structures with the blades and quasi-periodic or periodic emissions from the gearbox, generator, cooling fans, blade passage, and other moving components. These mechanical sources are easier to identify because they comprise of known, unique, periodic, and speed-dependent signatures. To identify potential mechanical sources, the time intervals between each acoustic event (i.e., spike) in each 32 s of data set were correlated with the average rotor speed, which only varies by ±3% in rated conditions, as shown earlier in Figure 4. The result is shown in Figure 14. Only data with at least six repeating spikes are shown to eliminate the influence of single, random spikes. Only 10% of the AEE data with any spikes met this criteria. In Figure 14, there is a cluster of spikes occurring near three orders (i.e., three per revolution of the main shaft), suggesting an influence of blade passage. As expected, there is limited evidence of events near 12.7 orders (i.e., the main bearing roller pass frequency for the outer ring), which confirms again that the bearing is healthy as indicated by the physical inspections. Although there are many other clusters of spikes shown in Figure 14, they do not correlate to known orders. This suggests that the influence from other components is limited. Figure 14 only illustrates situations with six or more repeating spike. The majority (i.e., 90%) of AEE data have either no spikes, less than six repeating spikes, or random spikes. Thus, the majority of AEE data likely contains many occurrences of asperity contacts in the main bearing.

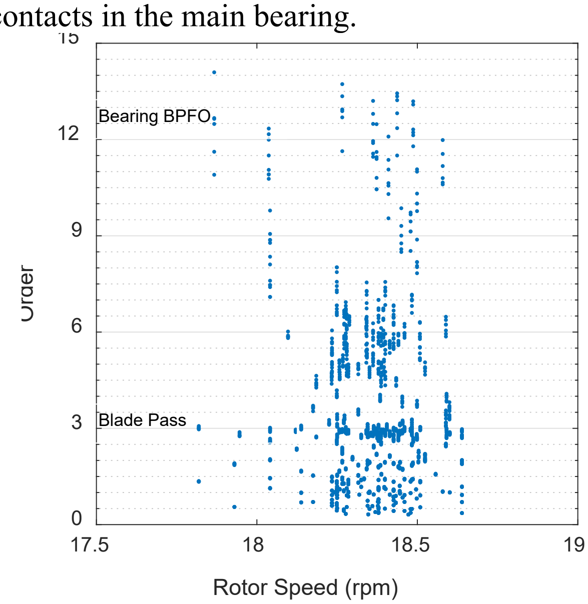

Figure 14. Identification of repeating acoustic events through order analysis

The percentage of periodic activities in the AEE data is further studied for various numbers of repeated intervals from 1 to 10. Figure 15 shows the number of feasible AEE spikes among all AEE data with up to ten interval repetitions. The number of filtered time intervals of acoustic events decreases sharply when the number of repeated intervals increases from 1 to 2, but levels off when it is greater than two. By estimating the curves elbow location at about 2.5 repeated intervals gives the percentage of periodic AEE activities that equals 11%, which matches the above estimation of 90% of random activity.

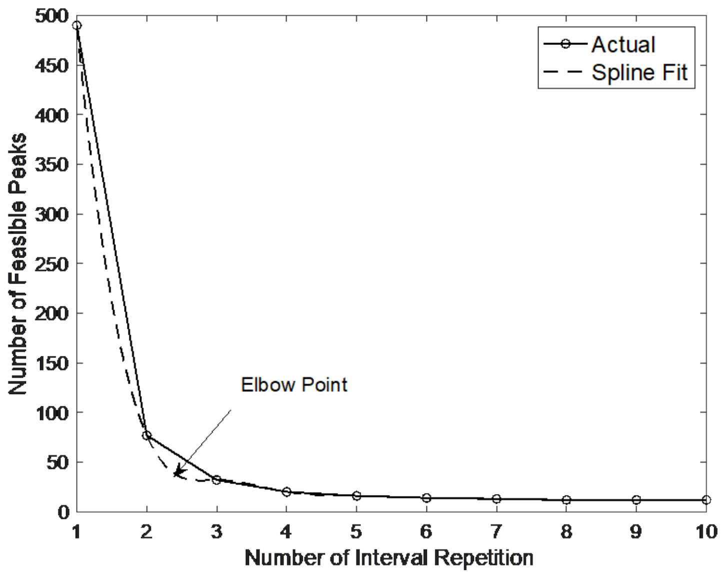

Figure 15. Variation in the number of feasible AEE peaks with number of interval repetitions

4 Conclusions and Future Work

This report described enveloped acoustic emissions and temperature characteristics of a newly installed, commercial main bearing in a wind turbine drivetrain. We measured these characteristics on the bearing outer ring by SKF DVST nodes and can be indicators of the bearing lubrication state. The measurements analyzed in this report span a five-month period between November 2018 and March 2019, around the end of the first year of bearing operation. The bearing and the grease had been visually inspected and were in good condition.

The presence of spikes and elevated RMS values of the enveloped acoustic emissions suggest that the lubricant film is insufficient to prevent asperity contacts in some conditions and/or that acoustic emissions from other sources are being measured. The correlations between multiple turbine operational parameters and the acoustic emission characteristics were also studied, including wind speed, rotor speed, bearing temperature, axial load, active power, and pitch activity. The acoustic emission characteristics were uniformly low below rated rotor speed. The highest enveloped acoustic emission characteristics were measured as follows:

- When the wind turbine was operating at the 14-m/s wind speed, at which the turbine is operating at rated rotor speed, rated power, rated torque, and actively pitching around 10 degrees. However, the axial load on the main bearing is lower in this condition than at the rated wind speed of 11 m/s.

- When the bearing was operating in hotter conditions of over 25°C as measured at the bottom of the generator side bearing row. This position was the hottest, as expected, because it is exposed to the highest combined axial and radial loads. The main bearing often operates in mixed lubrication conditions with estimated viscosity ratios of 0.5 to 2.3. The increased acoustic emission characteristics with temperature likely indicates a reduction in lubricant film thickness caused by a reduction in lubricant viscosity.

Preliminary study of emission sources from other wind turbine components, such as the blades and main bearing roller passage, indicates emissions resulting from the blade passage exist in 10% of the acoustic emission data. However, most of the acoustic emissions are random in nature and likely related to asperity contacts. Future work will be conducted to remove these influences and reexamine the correlation of acoustic emissions with turbine operating condition.

References

Beretta, M., A. Julian, J. Sepulveda, J. Cusidó, and O. Porro. 2021. "An Ensemble Learning Solution for Predictive Maintenance of Wind Turbines Main Bearing." *Sensors* 21(4): 1512. doi: 10.3390/s21041512.

Bergua Archeli, R., J. Keller, O. Bankestrom, M. Dunn, Y. Guo, A. Key, and E. Young. 2021. *Up-Tower Investigation of Main Bearing Cage Slip and Loads*. Golden, CO: National Renewable Energy Laboratory. NREL/TP-5000-81240. http://www.nrel.gov/docs/fy22osti/81240.pdf.

Brake, D. 2013. "WTG SRB Main Bearing Failures." Presented at UVIG Wind Turbine/Plant Operations & Maintenance Users Group Meeting.

Chovan, C. and A. J. Fierro. 2021. *Improving Bearing Life in Wind Turbine Main Shafts and Gearboxes*. The Timken Company. https://www.timken.com/resources/timken-tdi-bearings-white-paper-improving-bearing-life-in-wind-turbine-main-shafts-and-gearboxes/.

Cockerill, A., A. Clarke, R. Pullin, T. Bradshaw, P. Cole, and K. M. Holford. 2016. "Determination of Rolling Element Bearing Condition via Acoustic Emission." *Proceedings of the Institution of Mechanical Engineers, Part J: Journal of Engineering Tribology* 230(11): 1377–1388. doi: 10.1177/1350650116638612.

Cornel, D., F. Gutiérrez Guzmán, G. Jacobs, and S. Neumann. 2021. "Condition Monitoring of Roller Bearings Using Acoustic Emission." *Wind Energy Science* 6: 367–376. doi: 10.5194/wes-6-367-2021.

de Mello, E., G. Kampolis, E. Hart, D. Hickey, I. Dinwoodie, J. Carroll, R. Dwyer-Joyce, and A. Boateng. 2021. "Data Driven Case Study of a Wind Turbine Main-bearing Failure." *Journal of Physics: Conference Series* 2018: 012011. doi: 10.1088/1742-6596/2018/1/012011.

Fuentes, R., R. S. Dwyer-Joyce, M. B. Marshall, J. Wheals, E. J. Cross. 2020. "Detection of Sub-surface Damage in Wind Turbine Bearings Using Acoustic Emissions and Probabilistic Modelling." *Renewable Energy* 147(1): 776–797. doi: 10.1016/j.renene.2019.08.019.

Greco, A., S. Sheng, J. Keller, and A. Erdemir. 2013. "Material Wear and Fatigue in Wind Turbine Systems." *Wear* 302: 1583–1591. 10.1016/j.wear.2013.01.060.

Guo, Y., O. Bankestrom, R. Bergua, J. Keller, and M. Dunn. 2021. "Investigation of Main Bearing Operating Conditions in a Three-Point Mount Wind Turbine Drivetrain." *Forschung im Ingenieurwesen* 85: 405–421. 10.1007/s10010-021-00477-8.

Hart, E. 2020. "Developing a Systematic Approach to the Analysis of Time-varying Main Bearing Loads for Wind Turbines." *Wind Energy* 23(12): 2150–2165. 10.1002/we.2549.

Hart, E., A. Turnbull, J. Feuchtwang, D. McMillan, E. Golysheva, and R. Elliott. 2019. "Wind Turbine Main-Bearing Loading and Wind Field Characteristics." *Wind Energy* 22(11): 1534–1547. 10.1002/we.2386.

Hart, E., B. Clarke, G. Nicholas, A. Kazemi Amiri, J. Stirling, J. Carroll, R. Dwyer-Joyce, A. McDonald, and H. Long. 2020. "A Review of Wind Turbine Main Bearings: Design, Operation, Modelling, Damage Mechanisms and Fault Detection." *Wind Energy Science* 5: 105–124. 10.5194/wes-5-105-2020.

Hart, E., E. de Mello, and R. Dwyer-Joyce. 2022. "Wind Turbine Main-Bearing Lubrication – Part 1: An Introductory Review of Elastohydrodynamic Lubrication Theory." *Wind Energy Science* 7: 1021–1042. doi: 10.5194/wes-7-1021-2022.

Hart, E., E. de Mello, and R. Dwyer-Joyce. 2022. "Wind Turbine Main-Bearing Lubrication – Part 2: Simulation Based Results for a Double-row Spherical Roller Main-bearing in a 1.5 MW Wind Turbine." *Wind Energy Science* 7: 1533–1550. doi: 10.5194/wes-7-1533-2022.

Hart, E., A. Stock, G. Elderfield, R. Elliott, J. Brasseur, J. Keller, Y. Guo, and W. Song. 2022. "Impacts of Wind Field Characteristics and Non-steady Deterministic Wind Events on Time-varying Main-bearing Loads." *Wind Energy Science* 7: 1209–1226. doi: 10.5194/wes-7-1209-2022.

Hutt, S., A. Clarke, and H. P. Evans. 2018. "Generation of Acoustic Emission from the Running-in and Subsequent Micropitting of a Mixed-elastohydrodynamic Contact." *Tribology International* 119, 270–280. doi: 10.1016/j.triboint.2017.11.011.

Hase, A., H. Mishina, and M. Wada. 2012. "Correlation between Features of Acoustic Emission Signals and Mechanical Wear Mechanisms." *Wear* 292–293: 144–150. doi: 10.1016/j.wear.2012.05.019.

James, P. 2018. *Optimized Spherical Roller Bearing for Wind Turbine Rotors*. Presented at the Drivetrain Reliability Collaborative Meeting. February 21, 2018. https://www.dropbox.com/s/1vu6t47fovgaysh/03%20Optimized%20Spherical%20Roller%20Bearing.pdf?dl=0.

Keller, J., Y. Guo, and L. Sethuraman. 2019. *Uptower Investigation of Main and High-Speed-Shaft Bearing Reliability*. Golden, CO: National Renewable Energy Laboratory. NREL/TP-5000-71529. http://www.nrel.gov/docs/fy19osti/71529.pdf.

Keller, J., S. Sheng, Y. Guo, B. Gould, and A. Greco. 2021. *Wind Turbine Drivetrain Reliability and Wind Plant Operations and Maintenance Research and Development Opportunities*. Golden, CO: National Renewable Energy Laboratory. NREL/TP-5000-80195. http://www.nrel.gov/docs/fy21osti/80195.pdf.

Kotzalas, M. N. and G. L. Doll. 2010. "Tribological Advancements for Reliable Wind Turbine Performance." *Philosophical Transactions of the Royal Society A* 368: 4829–4850. 10.1098/rsta.2010.0194.

Nejad, A. R., J. Keller, Y. Guo, S. Sheng, H. Polinder, S. Watson, J. Dong, Z. Qin, A. Ebrahimi, R. Schelenz, et al. 2022. "Wind turbine drivetrains: state-of-the-art technologies and future development trends." *Wind Energy Science* 7: 387–411. 10.5194/wes-2021-63.

Raju, D. and O. Bankestrom. 2017. "A System Approach to Address Main Bearing Reliability." Presented at the Drivetrain Reliability Collaborative Meeting. February 21, 2018.

Santos, R., and J. van Dam. 2015. *Mechanical Loads Test Report for the U.S. Department of Energy 1.5-Megawatt Wind Turbine*. Golden, CO: National Renewable Energy Laboratory. NREL/TP-5000-63679. http://www.nrel.gov/docs/fy15osti/63679.pdf.

Sethuraman, L., Y. Guo, and S. Sheng, S. 2015. *Main Bearing Dynamics in Three-Point Suspension Drivetrains for Wind Turbines.* Golden, CO: National Renewable Energy Laboratory. NREL/PR-5000-64311. http://www.nrel.gov/docs/fy15osti/64311.pdf.

SKF. 2014. *Analysis and Interpretation of SKF Acoustic Emission Enveloping (AEE) Measurements*. Luleå, Sweden: SKF Condition Monitoring Center. CM3155 Application Note.

SKF. 2022a. "LGWM 2 High load, wide temperature grease." https://www.skf.com/us/products/lubrication-management/lubricants/high-load-wide-temperature.

SKF. 2022b. "240/600 BC Spherical roller bearings – SKF Explorer." https://www.skf.com/us/products/rolling-bearings/roller-bearings/spherical-roller-bearings/productid-240%2F600%20BC.

SKF. 2022c. "Lubrication condition – the viscosity ratio, *κ*" https://www.skf.com/us/products/rolling-bearings/principles-of-rolling-bearing-selection/bearing-selection-process/bearing-size/size-selection-based-on-rating-life/lubrication-condition-the-viscosity-ratio-k.